



Diurnal variations of BrONO₂ observed by MIPAS-B at mid-latitudes and in the Arctic

Gerald Wetzel¹, Hermann Oelhaf¹, Michael Höpfner¹, Felix Friedl-Vallon¹,
Andreas Ebersoldt², Thomas Gulde¹, Sebastian Kazarski¹, Oliver Kirner³,
5 Anne Kleinert¹, Guido Maucher¹, Hans Nordmeyer¹, Johannes Orphal¹,
Roland Ruhnke¹, and Björn-Martin Sinnhuber¹

¹Karlsruhe Institute of Technology, Institute of Meteorology and Climate Research, Karlsruhe, Germany

²Karlsruhe Institute of Technology, Institute for Data Processing and Electronics, Karlsruhe, Germany

³Karlsruhe Institute of Technology, Steinbuch Centre for Computing, Karlsruhe, Germany

10 *Correspondence to:* Gerald Wetzel (gerald.wetzel@kit.edu)

Abstract

The first stratospheric measurements of the diurnal variation of the inorganic bromine (Br_y)
reservoir species BrONO₂ around sunrise and sunset are reported. Arctic flights of the balloon-
borne Michelson Interferometer for Passive Atmospheric Sounding (MIPAS-B) were carried
15 out from Kiruna (68°N, Sweden) in January 2010 and March 2011 inside the stratospheric polar
vortices where diurnal variations of BrONO₂ around sunrise have been observed. High
nighttime BrONO₂ volume mixing ratios of up to 21 parts per trillion by volume (pptv) were
detected in the late winter 2011 in the absence of polar stratospheric clouds (PSCs). In contrast,
20 the amount of measured BrONO₂ was significantly lower in January 2010 due to low available
NO₂ amounts (for the build-up of BrONO₂), heterogeneous destruction of BrONO₂ on PSC
particles, and the gas-phase interaction of BrO (the source to form BrONO₂) with ClO. A further
balloon flight took place at mid-latitudes from Timmins (49°N, Canada) in September 2014.
Mean BrONO₂ mixing ratios of 22 pptv were observed after sunset in the altitude region
25 between 21 and 29 km. Measurements are compared and discussed with the results of a multi-
year simulation performed with the chemistry climate model ECHAM5/MESy Atmospheric
Chemistry (EMAC). The calculated temporal variation of BrONO₂ is in principal agreement
with the balloon-borne observations. Using the nighttime simulated ratio between BrONO₂ and
Br_y, the amount of Br_y observed by MIPAS-B was estimated to about 21-25 pptv in the lower
30 stratosphere.



1 Introduction

Chlorine and bromine species play a dominant role in the contribution to ongoing stratospheric ozone depletion since the amount of equivalent effective stratospheric chlorine (chlorine and bromine) is predicted to return to 1980 values by 2050 at mid-latitudes (Newman et al., 2007; 35 Stolarski et al., 2010). BrONO₂ is, besides BrO, the most abundant inorganic bromine (Br_y) compound in the stratosphere (see e.g. Brasseur and Solomon, 2005; Sinnhuber et al., 2009; Sinnhuber and Meul, 2015). BrONO₂ is formed via the reaction with BrO and NO₂:



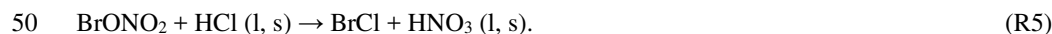
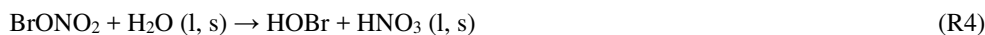
During day, BrONO₂ is photolyzed with different possible channels



with a higher quantum yield of (R2a) compared to (R2b). BrONO₂ can also be destroyed via the reaction with atomic oxygen:



45 (R1) to (R3) exhibit the close connection between BrO and BrONO₂ leading to an opposite diurnal variation of these species. Gas-phase BrONO₂ can also be converted to gas-phase HOBr and BrCl on sulphate aerosols and polar stratospheric cloud (PSC) particles where H₂O, HCl, and HNO₃ are in liquid (l) or solid phase (s):



An interaction between the chlorine and bromine family (particularly important at high latitudes in winter under conditions of elevated ClO) is the gas-phase production of BrCl via:



Stratospheric BrONO₂ was detected for the first time by the Michelson Interferometer for 55 Passive Atmospheric Sounding (MIPAS) aboard the Envisat satellite (Höpfner et al., 2009). Strong day/night variations were observed with much lower concentrations during day compared to nighttime. A maximum amount of 20-25 pptv (parts per trillion by volume) was inferred from MIPAS spectra recorded during the night.



Flights of the balloon version of the MIPAS instrument (MIPAS-B) investigated in this work
60 were carried out from Kiruna (68°N, Sweden) on 24 January 2010 and 31 March 2011 as well
as from Timmins (49°N, Canada), on 7/8 September 2014. For the first time, diurnal variations
of BrONO₂ around sunrise (Kiruna flights) and sunset (Timmins flight) were measured by
MIPAS-B with high temporal resolution. A description of the MIPAS-B instrument, data
analysis and chemical modelling is given in Sect. 2. A discussion of observed BrONO₂ volume
65 mixing ratio (VMR) vertical profiles follows in Sect. 3 together with a comparison of the
measured data to simulations of the chemistry climate model ECHAM5/MESSEy Atmospheric
Chemistry (EMAC) to check the current understanding of stratospheric bromine chemistry and
to estimate the amount of lower stratospheric Br_y.

70 2 MIPAS-B instrument, data analysis and modelling

In the following sections, we give an overview of the MIPAS-B instrument and the balloon
flights together with the corresponding data analysis and a description of chemical modelling
performed for this study.

2.1 MIPAS-B instrument and balloon flights

75 The balloon-borne cryogenic Fourier Transform limb emission spectrometer operates in the
mid-infrared spectral region between about 4 and 14 μm. The maximum optical path difference
of 14.5 cm of the beam in the interferometer correlates with 0.0345 cm⁻¹ spectral resolution.
This corresponds to about 0.07 cm⁻¹ after apodization with the Norton and Beer (1976) “strong”
function and allows the separation of individual spectral lines from continuum-like emissions.
80 Noise equivalent spectral radiance (NESR) values for a single calibrated spectrum are typically
within 1x10⁻⁹ and 7x10⁻⁹ W(cm² sr cm⁻¹)⁻¹. A reduction of spectral noise by a factor of $n^{0.5}$ is
obtained by recording and averaging of n spectra ($n \leq 16$) per single elevation scan. Besides a
high radiometric accuracy of typically 1%, the pointing system allows a knowledge of the
tangent altitude of better than 50 m at the 1-σ confidence limit. An overview of instrument
85 characterization in terms of the instrumental line shape, field of view, NESR, line of sight of
the instrument, detector non-linearity (Kleinert, 2006) and the error assessment of the calibrated
spectra is given by Friedl-Vallon et al. (2004).

In this study, we report BrONO₂ results from three MIPAS-B flights. Details are shown in Table
1. The first flight took place on 24 January 2010 from Kiruna over northern Scandinavia inside



90 the Arctic vortex at the beginning of a major stratospheric warming (Wetzel et al., 2012). The
second one was carried out from the same location on 31 March 2011 inside a still persistent
late-winter Arctic vortex (Wetzel et al., 2015). The third one was performed at mid-latitudes
from Timmins (Ontario, Canada) on 7 to 8 September 2014. For this mid-latitude flight, we
show retrieval results from spectra observed around sunset. For the Arctic flights, MIPAS-B
95 measurements were performed from night into day. All flights have in common that fast
sequences of spectra were recorded in short time steps of about 10 min to enable the retrieval
of photochemically active species, which change quickly their concentration around sunrise and
sunset. The line of sight of the instrument was aligned perpendicular to the azimuth direction
of the sun to allow for a symmetric illumination of the sounded air mass before and beyond the
100 tangent point. The analysis of the recorded spectra is described in the following section.

2.2 Data analysis

Radiance calculations were carried out with the Karlsruhe Optimized and Precise Radiative
transfer Algorithm (KOPRA; Stiller et al., 2002). Spectroscopic parameters for the calculation
of emission spectra were taken from the high-resolution transmission molecular absorption
105 database (HITRAN; Rothman et al., 2009) and a MIPAS dedicated line list (Raspollini et al.,
2013). Spectral features of the molecule BrONO₂ were calculated using new pressure-
temperature dependent absorption cross sections measured by Wagner and Birk (2016) with a
2% intensity accuracy. KOPRA also provides derivatives of the radiance spectrum with respect
to atmospheric state and instrument parameters (Jacobians) which are used by the retrieval
110 procedure KOPRAFIT (Höpfner et al., 2002). The vertical distance of tangent altitudes ranges
between 1 and 1.5 km. Thus, the retrieval grid was set to 1 km up to the balloon float (observer)
altitude. Above this level, the vertical spacing increases gradually up to 10 km at the top altitude
of 100 km. Considering the smoothing of the vertical part of the instrumental field of view, the
retrieval grid is somewhat finer than the achievable vertical resolution of the measurement for
115 most parts of the altitude region covered (especially above the observer altitude). To avoid
retrieval instabilities caused by this oversampling, a Tikhonov-Phillips regularization approach
(Phillips, 1962; Tikhonov, 1963) was applied using a constraint with respect to a first derivative
of the a priori profile \mathbf{x}_a of the target species:

$$\mathbf{x}_{i+1} = \mathbf{x}_i + [\mathbf{K}_i^T \mathbf{S}_y^{-1} \mathbf{K}_i + \mathbf{R}]^{-1} [\mathbf{K}_i^T \mathbf{S}_y^{-1} (\mathbf{y}_{\text{meas}} - \mathbf{y}(\mathbf{x}_i)) - \mathbf{R}(\mathbf{x}_i - \mathbf{x}_a)], \quad (1)$$



120 where \mathbf{x}_{i+1} is the vector of the state parameters \mathbf{x}_i for iteration $i+1$; \mathbf{y}_{meas} is the measured radiance vector and $\mathbf{y}(\mathbf{x}_i)$ the calculated radiance using state parameters of iteration i ; \mathbf{K} is the Jacobian matrix with partial derivatives $\partial \mathbf{y}(\mathbf{x}_i) / \partial \mathbf{x}_i$ while \mathbf{S}_y^{-1} is the inverse noise measurement covariance matrix and \mathbf{R} a regularization matrix composed of the first derivative operator and a regularization strength parameter.

125 The BrONO₂ retrieval calculations were performed in the range of the ν_3 band centred at 803.37 cm⁻¹. Figure 1 shows spectral contributions of relevant species in the BrONO₂ microwindow from 801 to 820 cm⁻¹ that has been found best appropriate to derive the BrONO₂ amount from MIPAS-B spectra. Besides the target molecule BrONO₂, all main interfering species H₂O, CO₂, O₃, NO₂, HNO₃, COF₂, HCFC-22 (CHClF₂), CCl₄, CFC-113 (C₂Cl₃F₃), ClONO₂, HO₂NO₂, and
130 PAN (peroxyacetyl nitrate) were fitted simultaneously together with temperature, instrumental offset and wavenumber shift. The molecule HO₂NO₂ shows a similar spectral band shape like the target species BrONO₂. Since the HO₂NO₂ absorption cross sections (included in HITRAN) measured by May and Friedl (1993) are derived at only one temperature (220 K) a second set of cross sections derived by Friedl et al. (1994) at room temperature (298 K) was used to allow
135 a two-point interpolation of the cross section intensity to the current atmospheric temperature.

Vertical profiles of minor contributing species were either adjusted in appropriate microwindows prior to the BrONO₂ retrieval or taken from a climatological atmosphere (Remedios et al., 2007), updated with surface concentration data from NOAA ESRL GMD (National Oceanic and Atmospheric Administration, Earth System Research Laboratory,
140 Global Monitoring Division; Montzka et al., 1999). An example of a best fit of a measured MIPAS-B spectrum zoomed around the Q-branch region of the BrONO₂ ν_3 band for a tangent altitude near 20 km is shown in Figure 2. The spectrum was recorded during night. If the fit is performed in absence of BrONO₂ in the model atmosphere, a systematic residual is remaining around the centre of the BrONO₂ Q-branch at 803.37 cm⁻¹ (blue solid line in Figure 2). If the
145 molecule BrONO₂ is taken into account by the radiative transfer calculation, the systematic residual around the Q-branch disappears demonstrating the existence of BrONO₂ in the stratosphere. Another example for a best fit in the same altitude region but for a MIPAS-B spectrum recorded during day is illustrated in Figure 3. Here, we recognize that for a daytime situation the effect whether the species BrONO₂ is included in the radiative transfer calculations
150 or not, is clearly smaller compared to the nighttime case (cf. Figure 2) such that we expect lower stratospheric BrONO₂ VMRs during day and higher values at night. This is confirmed by the



retrieved vertical profiles of BrONO₂ illustrated in Figures 4 and 5 together with the error budget and altitude resolution. The dominant part of the total error in the BrONO₂ retrieval is spectral (random) noise resulting in a BrONO₂ VMR error of about 2 to 4 pptv (10-25%) in the
155 altitude region of the VMR maximum. An important systematic error source are uncertainties of disturbing gases overlapping the BrONO₂ ν₃ band. This influence was estimated using uncertainties in line intensity and half-width as given by Flaud et al. (2003) and HITRAN (Rothman et al., 2009) and results into a BrONO₂ error of up to 2 pptv (10-20%) in the altitude region of the BrONO₂ VMR maximum. Retrieval simulations of the major interfering species
160 O₃, CO₂, and H₂O have revealed an influence (line half-width and intensity uncertainties) within 10% on the BrONO₂ amount (Höpfner et al., 2009). The species ClONO₂, followed by HO₂NO₂ have large contributions to the limb emission spectra (see Figure 1). Temperature and pressure dependent ClONO₂ absorption cross sections were measured by Wagner and Birk (2003) with high accuracy. Systematic errors in the BrONO₂ VMR due to ClONO₂ spectroscopy are
165 expected to be within 10% (Wagner and Birk, 2016). As mentioned above, a temperature dependence of HO₂NO₂ absorption cross sections was included to improve spectroscopy of this interfering species. Further systematic error sources like radiometric gain, line of sight, and the spectroscopy of the target molecule BrONO₂ itself are of minor importance for the total error budget of the BrONO₂ retrieval (see Figures 4 and 5). The altitude resolution of the retrieved
170 BrONO₂ profiles amounts to between about 4 and 6 km (~ 4-5 degrees of freedom) over a wide range in the stratosphere.

2.3 Model calculations

Measured MIPAS-B data are compared to a multi-year simulation of the chemistry climate model EMAC that includes sub-models describing tropospheric and middle atmosphere
175 processes (Jöckel et al., 2010). The core atmospheric model is the 5th generation European Centre Hamburg general circulation model (ECHAM5; Roeckner et al., 2006) which is linked to the sub-models via the interface Modular Earth Submodel System (MESSy). For the present study we applied EMAC (ECHAM5 version 5.3.02, MESSy version 2.52) in the T42L90MA-resolution, i.e., with a spherical truncation of T42 (corresponding to a Gaussian grid of
180 approximately 2.8 by 2.8 degrees in latitude and longitude) and 90 vertical hybrid pressure levels from the ground up to 0.01 hPa (approx. 80 km). The calculation of gas-phase chemistry is realized by the submodel MECCA (Sander et al., 2005). The submodel MSBM (Kirner et al., 2011) simulates polar stratospheric clouds and calculates heterogeneous reaction rates.



A Newtonian relaxation technique of the surface pressure and the prognostic variables
185 temperature, vorticity, and divergence above the boundary layer and below 1 hPa towards the
ECMWF reanalysis ERA-Interim (Dee et al., 2011) has been applied to simulate realistic
synoptic conditions (van Aalst, 2005). The simulation includes a comprehensive chemistry
setup from the troposphere to the lower mesosphere with more than 100 species involved in gas
phase-, photolysis-, and heterogeneous reactions on liquid sulphate aerosols, nitric acid
190 trihydrate (NAT) and ice particles. Rate constants of gas-phase reactions originate from
Atkinson et al. (2007) and the Jet Propulsion Laboratory (JPL) compilation (Sander et al.,
2011). Photochemical reactions of short-lived bromine-containing organic compounds CH_3Br ,
 CHBr_3 , CH_2Br_2 , CH_2ClBr , CHClBr_2 , and CHCl_2Br are integrated into the model setup (Jöckel
et al., 2016). Surface emissions of these species are taken from scenario 5 of Warwick et al.
195 (2006). During the time period with MIPAS-B balloon flights the model output data were saved
every 10 minutes. The temporally closest model output to the MIPAS-B measurements was
interpolated in space to the observed geolocations.

3 Results and discussion

200 In this section, vertical profiles retrieved from MIPAS-B limb emission spectra measured
before and after sunrise (Arctic flights) and sunset (mid-latitude flight) are shown. The
measured data have been temporally smoothed with a 3-point adjacent averaging routine to
attenuate noisy structures. These data were compared to EMAC simulations. To permit a more
realistic comparison with respect to different altitude resolutions in the measurement and the
205 simulation, EMAC vertical profiles were additionally smoothed with the averaging kernel
matrix and the a priori profile of MIPAS-B. A smoothed EMAC profile \mathbf{x}_s is calculated
following the method described in Rodgers (2000):

$$\mathbf{x}_s = \mathbf{x}_a + \mathbf{A}(\mathbf{x} - \mathbf{x}_a^*), \quad (2)$$

where \mathbf{x}_a is the a priori profile of MIPAS-B, \mathbf{x}_a^* the a priori profile interpolated to the altitude
210 grid of the EMAC profile \mathbf{x} , and \mathbf{A} is the averaging kernel matrix of MIPAS-B.

3.1 Arctic measurements

The temporal evolution of BrONO_2 measured during the balloon flight from Kiruna on 31
March 2011 inside the late winter stratospheric polar vortex is shown in Figure 6. No PSCs



were present during the time of the MIPAS-B measurement (Wetzel et al., 2015). A nighttime
215 maximum of BrONO₂ around 25 km with values of more than 20 pptv is clearly visible. After
sunrise, the amount of BrONO₂ decreases to maximum values of about 14 pptv around 22 km.
The corresponding EMAC simulation is depicted in Figure 7. The overall structure of the
simulated temporal evolution of BrONO₂ is similar to the measured one. Maximum nighttime
BrONO₂ values in EMAC are comparable to the measured amounts. However, above the
220 nocturnal VMR maximum, EMAC calculates higher BrONO₂ concentrations compared to the
balloon observation. Furthermore, the daytime photochemical destruction of BrONO₂ is
slightly faster in the model yielding several pptv lower daytime BrONO₂ VMRs in the model
compared to MIPAS-B. A sensitivity study performed by Kreygy et al. (2013) indicates that
very likely the BrONO₂ photolysis rate and the reaction rate of the BrONO₂ build-up from BrO
225 and NO₂ differs from the JPL recommendation that was also used in EMAC. However, their
study refers to stratospheric mid-latitude conditions and the outcome is therefore not directly
comparable to the Arctic observations shown here. The EMAC simulation smoothed with the
averaging kernel matrix of MIPAS-B according to Eq. (2) is displayed in Figure 8. A main
difference to the unsmoothed case shown in Figure 7 is the reduction of the nighttime BrONO₂
230 VMR at altitudes above the maximum that yields to a better agreement with measured BrONO₂.
During night, a large part of lower stratospheric inorganic bromine is in the form of BrONO₂.
This gives the opportunity to estimate the amount of “measured” inorganic bromine [Br_y(meas)]
from measured nighttime [BrONO₂(meas)] using the calculated [BrONO₂(mod)]/[Br_y(mod)]
ratio from EMAC in the following form:

$$235 \quad [\text{Br}_y(\text{meas})] = \frac{[\text{BrONO}_2(\text{meas})][\text{Br}_y(\text{mod})]}{[\text{BrONO}_2(\text{mod})]}. \quad (3)$$

Applying Eq. (3) for a nighttime (SZA ≥ 96°) ratio [BrONO₂(mod)]/[Br_y(mod)] ≥ 0.8
corresponding to an altitude region between 23 and 29 km we calculate [Br_y(meas)] (including
the total [BrONO₂(meas)] error) to 22.3 ± 2.2 pptv. The given error bar represents the 1-σ total
240 error originating from measured BrONO₂.

Another Arctic balloon flight was performed from Kiruna on 24 January 2010 inside a cold
polar vortex under mid-winter weak illumination conditions. As a consequence of low
stratospheric temperatures in this winter, widespread PSCs were present in an altitude region
between about 18 and 24 km at the time of the MIPAS-B observation (Wetzel et al., 2012). The



245 observed BrONO₂ as seen from night until noon is shown in Figure 9. Nighttime BrONO₂
mixing ratios are clearly lower compared to the previously discussed situation in late March
2011. This is also reflected in the EMAC simulation (Figure 10). During the long polar night
the amount of available NO₂ (Wetzel et al. 2012) to produce BrONO₂ via (R1) is significantly
reduced due to the conversion of NO₂ into its reservoir species (mainly HNO₃). In this period
250 of darkness, nearly all BrONO₂ below 25 km (PSC region) is converted to BrCl via
heterogeneous chemistry according to (R5) and gas-phase conversion of BrO to BrCl via (R6).
Here, more than 90 % of Br_y are in the form of BrCl in the model simulation during night.
Above this altitude region, BrONO₂ and BrCl together are the dominant species of the nocturnal
Br_y budget in the EMAC run. During day, photolysis of both species (BrONO₂ and BrCl)
255 leads to an increase of BrO such that this species then dominates the Br_y budget. If we smooth
the EMAC BrONO₂ data with the averaging kernel matrix of MIPAS-B, we see a better
agreement with MIPAS-B in the structure of the temporal evolution of the BrONO₂ amount
(Figure 11). The effect of the smoothing appears to be stronger compared to the case in March
2011 since low temperatures together with low amounts of BrONO₂ in January 2010 entailed
260 to perform the retrieval with a factor of 2 coarser altitude resolution compared to a standard
BrONO₂ retrieval setup as depicted in Figures 4 and 5.

3.2 Mid-latitude measurements

MIPAS-B spectra have been recorded from day until night over Ontario (Canada) during a
balloon flight launched from Timmins on 7 September 2014. The temporal evolution of
265 measured BrONO₂ is depicted in Figure 12. A significant increase of BrONO₂ starting shortly
before sunset is visible. This is caused by the weakened illumination at SZAs near 90° that
enables the build-up of BrONO₂ from daytime BrO via (R1). Nighttime BrONO₂ mixing ratios
of more than 24 pptv are seen by MIPAS-B around 28 km altitude. The corresponding EMAC
model simulation is displayed in Figure 13. The principal shape of the increase of BrONO₂
270 VMR is reproduced by the model run although absolute values are somewhat lower in the
simulation compared to the measurement. Differences in absolute BrONO₂ amounts are at least
partly connected with the fact that EMAC NO₂ values are up to 20 % lower than the observed
NO₂ in the altitude region of the BrONO₂ VMR maximum. The BrONO₂ increase in the model
starts earlier compared to the measurement. Nighttime maximum BrONO₂ values in EMAC
275 reach about 22 pptv and are located in the same altitude region as seen in the observation.
Smoothing the EMAC data with the averaging kernel matrix of MIPAS-B yields to a better



agreement with the structure of the observational data at altitudes below about 18 km (Figure 14).

280 During night, more than 90 % of simulated mid-litudinal lower stratospheric inorganic bromine is in the form of BrONO₂. Hence, we again apply Eq. (3) to estimate “measured” inorganic bromine. In an altitude region between 21 and 29 km, corresponding to a nighttime (SZA ≥ 99°) ratio [BrONO₂(mod)]/[Br_y(mod)] ≥ 0.9, we then calculate [Br_y(meas)] to 23.6 ± 1.9 pptv.

285 4 Conclusions

BrONO₂ observations around sunrise were performed during balloon flights with MIPAS-B carried out in the Arctic from Kiruna on 24 January 2010 and 31 March 2011 and at mid-latitudes from Timmins on 7/8 September 2014. Measured BrONO₂ diurnal variations with high nighttime and low daytime values confirm the stratospheric bromine chemistry (introduced 290 in Sect. 1) that is dominated by the interaction of BrO and BrONO₂ according to (R1) – (R3). During polar winter (January 2010) with weak illumination, large parts of nighttime Br_y are in the form of BrCl resulting in significantly lower BrONO₂ values compared to the situation in late Arctic winter (March 2011) and mid-latitude summer (September 2014).

The chemistry climate model EMAC is able to reproduce the temporal variation of the measured 295 BrONO₂ values. However, some differences in the absolute amounts of BrONO₂ are obvious. The simulated BrONO₂ mixing ratios are dependent on the assumed total Br_y in the model, which amounts about 23 pptv in the lower stratosphere. As mentioned in Sect. 2.3 reactions of short-lived bromine-containing organic compounds are integrated into the model setup according to emission scenarios shown by Warwick et al. (2006). This is equivalent to about 6- 300 7 pptv inorganic bromine from these oceanic short-lived bromocarbons in the upper troposphere.

As discussed in Sect. 3, Br_y in the lower stratosphere was estimated from MIPAS-B measurements. For the Arctic observation in March 2011, we obtain 22.3 ± 2.2 pptv Br_y and for the mid-latitude measurement in September 2014, we calculate 23.6 ± 1.9 pptv Br_y in the 305 lower stratosphere. These values can be compared to observations of stratospheric Br_y calculated with photochemical modelling using balloon-borne direct sun DOAS (Differential Optical Absorption Spectroscopy) BrO observations (Dorf et al., 2006; Carpenter et al., 2014)



and annual mean mixing ratios derived from ground-based UV-visible measurements of stratospheric BrO (Sinnhuber et al., 2002; Hendrick et al., 2007; Hendrick et al., 2008; 310 Carpenter et al., 2014). These observations show the temporal development of Br_y in dependence of the year when air masses are entering the stratosphere. Assuming a mean age of air of 6 years at 25 km (Haenel et al., 2015) we can compare the measured Br_y from MIPAS-B directly to the Br_y from DOAS observations in the years (of stratospheric entry) 2005 and 2008. In these years, the range of expected Br_y spans from about 18 to 25 pptv taking into account the 315 error limits. Although the amount of Br_y inferred from MIPAS-B measurements lies more towards the upper edge of this range, it is still consistent with the Br_y estimates from DOAS observations.

Finally, it should be mentioned that there is still some limited potential on the improvement of the spectroscopy of the interfering species (mainly HO₂NO₂) in the BrONO₂ spectral analysis 320 window (Wagner and Birk, 2016). However, BrONO₂ test retrieval simulations for MIPAS-B (within this work) and MIPAS (Höpfner et al., 2009) have shown that future improvements in the spectroscopic database will most probably not exceed the total error limits given in this study.

325 **Acknowledgements**

We are grateful to the CNES balloon team for excellent balloon operations and the Swedish Space Corporation for operating Arctic campaigns and logistical assistance. We thank Katja Grunow from Free University of Berlin for meteorological support. The work presented here was funded in part by the European Space Agency (ESA) and the German Aerospace Center 330 (DLR). We acknowledge support by Deutsche Forschungsgemeinschaft and Open Access Publishing Fund of Karlsruhe Institute of Technology.



References

- Atkinson, R., Baulch, D. L., Cox, R. A., Crowley, J. N., Hampson, R. F., Hynes, R. G., Jenkin,
335 M. E., Rossi, M. J., and Troe, J.: Evaluated kinetic and photochemical data for atmospheric
chemistry: Volume III – gas phase reactions of inorganic halogens, *Atmos. Chem. Phys.*, 7,
981-1191, doi:10.5194/acp-7-981-2007, 2007.
- Brasseur, G., and Solomon, S.: *Aeronomy of the middle atmosphere* (third edition), *Atmos.
Oceanograph. Sci. Lib.*, p. 369 ff, Springer, Dordrecht, The Netherlands, 2005.
- 340 Carpenter, L. J., Reimann, S., Burkholder, J. B., Clerbaux, C., Hall, B. D., Hossaini, R., Laube,
J. C., and Yvon-Lewis, S. A.: Ozone-Depleting Substances (ODSs) and other gases of
interest to the Montreal Protocol, Chapter 1 in *Scientific Assessment of Ozone Depletion:
2014, Global Ozone Research and Monitoring Project – Report No. 55*, 416 pp., World
Meteorological Organization, Geneva, Switzerland, 2014.
- 345 Dee, D. P., Uppala, S. M., Simmons, A. J., Berrisford, P., Poli, P., Kobayashi, S., Andrae, U.,
Balmaseda, M. A., Balsamo, G., Bauer, P., Bechtold, P., Beljaars, A. C. M., van de Berg, L.,
Bidlot, J., Bormann, N., Delsol, C., Dragani, R., Fuentes, M., Geer, A. J., Haimberger, L.,
Healy, S. B., Hersbach, H., Hólm, E. V., Isaksen, L., Kållberg, P., Köhler, M., Matricardi,
M., McNally, A. P., Monge-Sanz, B. M., Morcrette, J.-J., Park, B.-K., Peubey, C., deRosnay,
350 P., Tavolato, C., Thépaut, J.-N., F. Vitart, F.: The ERA-Interim reanalysis: configuration and
performance of the data assimilation system, *Q. J. R. Meteorol. Soc.* 137, 553 – 597, 2011.
- Dorf, M., Butler, J. H., Butz, A., Camy-Peyret, C., Chipperfield, M. P., Kritten, L., Montzka,
S. A., Simmes, B., Weidner, F., and Pfeilsticker, K.: Long-term observations of stratospheric
bromine reveal slow down in growth, *Geophys. Res. Lett.*, 33, L24803,
355 doi:10.1029/2006GL027714, 2006.
- Flaud, J.-M., Piccolo, C., Carli, B., Perrin, A., Coudert, L.H., Teffo, J.-L., and Brown, L.R.:
Molecular line parameters for the MIPAS (Michelson Interferometer for Passive
Atmospheric Sounding) experiment, *Atmos. Oceanic Opt.*, 16, 172-182, 2003.
- Friedl, R. R., May, R. D., and Duxbury, G.: The ν_6 , ν_7 , ν_8 , and ν_{10} bands of HO_2NO_2 , *J. Mol.*
360 *Spectrosc.*, 165, 481-493, 1994.
- Friedl-Vallon, F., Maucher, G., Kleinert, A., Lengel, A., Keim, C., Oelhaf, H., Fischer, H.,
Seefeldner, M., and Trieschmann, O.: Design and characterization of the balloon-borne



- Michelson Interferometer for Passive Atmospheric Sounding (MIPAS-B2), *Appl. Opt.*, 43, 3335-3355, 2004.
- 365 Haedel, F. J., Stiller, G. P., von Clarmann, T., Funke, B., Eckert, E., Glatthor, N., Grabowski, U., Kellmann, S., Kiefer, M., Linden, A., and Reddman, T.: Reassessment of MIPAS age of air trends and variability, *Atmos. Chem. Phys.*, 15, 13161–13176, doi:10.5194/acp-15-13161-2015, 2015.
- Hendrick, F., Van Roozendaal, M., Chipperfield, M. P., Dorf, M., Goutail, F., Yang, X., Fayt, 370 C., Hermans, C., Pfeilsticker, K., Pommereau, J.-P., Pyle, J. A., Theys, N., and De Mazière, M.: Retrieval of stratospheric and tropospheric BrO profiles and columns using ground-based zenith-sky DOAS observations at Harestua, 60° N, *Atmos. Chem. Phys.*, 7, 4869-4885, doi:10.5194/acp-7-4869-2007, 2007.
- Hendrick, F., Johnston, P. V., De Mazière, M., Fayt, C., Hermans, C., Kreher, K., Theys, N., 375 Thomas, A., and Van Roozendaal, M.: One-decade trend analysis of stratospheric BrO over Harestua (60°N) and Lauder (45°S) reveals a decline, *Geophys. Res. Lett.*, 35, L14801, doi:10.1029/2008GL034154, 2008.
- Höpfner, M., Oelhaf, H., Wetzel, G., Friedl-Vallon, F., Kleinert, A., Lengel, A., Maucher, G., Nordmeyer, H., Glatthor, N., Stiller, G., von Clarmann, T., Fischer, H., Kröger, C., and 380 Deshler, T.: Evidence of scattering of tropospheric radiation by PSCs in mid-IR limb emission spectra: MIPAS-B observations and KOPRA simulations, *Geophys. Res. Lett.*, 29(8), 1278, doi:10.1029/2001GL014443, 2002.
- Höpfner, M., Orphal, J., von Clarmann, T., Stiller, G., and Fischer, H.: Stratospheric BrONO₂ observed by MIPAS, *Atmos. Chem. Phys.*, 9, 1735–1746, doi:10.5194/acp-9-1735-2009, 385 2009.
- Jöckel, P., Kerkweg, A., Pozzer, A., Sander, R., Tost, H., Riede, H., Baumgaertner, A., Gromov, S., and Kern, B.: Development cycle 2 of the Modular Earth Submodel System (MESSy2), *Geosci. Model Dev.*, 3, 717-752, doi:10.5194/gmd-3-717-2010, 2010.
- Jöckel, P., Tost, H., Pozzer, A., Kunze, M., Kirner, O., Brenninkmeijer, C. A. M., Brinkop, S., 390 Cai, D. S., Dyroff, C., Eckstein, J., Frank, F., Garny, H., Gottschaldt, K.-D., Graf, P., Grewe, V., Kerkweg, A., Kern, B., Matthes, S., Mertens, M., Meul, S., Neumaier, M., Nützel, M., Oberländer-Hayn, S., Ruhnke, R., Runde, T., Sander, R., Scharffe, D., and Zahn, A.: Earth System Chemistry integrated Modelling (ESCiMo) with the Modular Earth Submodel



- 395 System (MESSy) version 2.51, *Geosci. Model Dev.*, 9, 1153-1200, doi:10.5194/gmd-9-1153-2016, 2016.
- Kirner, O., Ruhnke, R., Buchholz-Dietsch, J., Jöckel, P., Brühl, C., and Steil, B.: Simulation of polar stratospheric clouds in the chemistry-climate-model EMAC via the submodel PSC, *Geosci. Model Dev.*, 4, 169-182, doi:10.5194/gmd-4-169-2011, 2011.
- Kleinert, A.: Correction of detector nonlinearity for the balloonborne Michelson Interferometer
400 for Passive Atmospheric Sounding, *Appl. Opt.*, 45, 425-431, 2006.
- Kreycy, S., Camy-Peyret, C., Chipperfield, M. P., Dorf, M., Feng, W., Hossaini, R., Kritten, L., Werner, B., and Pfeilsticker, K.: Atmospheric test of the $J(\text{BrONO}_2)/k_{\text{BrO}+\text{NO}_2}$ ratio: implications for total stratospheric Br_y and bromine-mediated ozone loss, *Atmos. Chem. Phys.*, 13, 6263–6274, doi:10.5194/acp-13-6263-2013, 2013.
- 405 May, R. D., and Friedl, R. R.: Integrated band intensities of HO_2NO_2 at 220 K, *J. Quant. Spectrosc. Radiat. Transfer*, 50, 257-266, 1993.
- Montzka, S. A., Butler, J. H., Elkins, J. W., Thompson, T. M., Clarke, A. D. and Lock, L. T.: Present and future trends in the atmospheric burden of ozone-depleting halogens, *Nature*, 398, 690-694, 1999.
- 410 Newman, P. A., Daniel, J. S., Waugh, D. W., and Nash, E. R.: A new formulation of equivalent effective stratospheric chlorine (EESC), *Atmos. Chem. Phys.*, 7, 4537–4552, doi:10.5194/acp-7-4537-2007, 2007.
- Norton, H., and Beer, R.: New apodization functions for Fourier spectroscopy, *J. Opt. Soc. Am.*, 66, 259-264 (Errata, *J. Opt. Soc. Am.*, 67, 419, 1977.) 1976.
- 415 Phillips, D.: A technique for the numerical solution of certain integral equations of the first kind, *J. Assoc. Comput. Math.*, 9, 84–97, 1962.
- Raspollini, P., Carli, B., Carlotti, M., Ceccherini, S., Dehn, A., Dinelli, B. M., Dudhia, A., Flaud, J.-M., López-Puertas, M., Niro, F., Remedios, J. J., Ridolfi, M., Sembhi, H., Sgheri, L., and von Clarmann, T.: Ten years of MIPAS measurements with ESA Level 2 processor
420 V6 – Part 1: Retrieval algorithm and diagnostics of the products, *Atmos. Meas. Tech.*, 6, 2419-2439, doi:10.5194/amt-6-2419-2013, 2013.
- Remedios, J. J., Leigh, R. J., Waterfall, A. M., Moore, D. P., Sembhi, H., Parkes, I., Greenhough, J., Chipperfield, M. P., and Hauglustaine, D.: MIPAS reference atmospheres



- and comparisons to V4.61/V4.62 MIPAS level 2 geophysical data sets, *Atmos. Chem. Phys. Discuss.*, 7, 9973–10017, doi:10.5194/acpd-7-9973-2007, 2007.
- 425
- Rodgers, C.: *Inverse methods for atmospheric sounding: Theory and practice*, World Sci., Hackensack, N. J., 2000.
- Roeckner, E., Brokopf, R., Esch, M., Giorgetta, M., Hagemann, S., Koernblueh, L., Manzini, E., Schlese, U., and Schulzweida, U.: Sensitivity of simulated climate to horizontal and vertical resolution in the ECHAM5 atmosphere model, *J. Climate*, 19, 3771–3791, 2006.
- 430
- Rothman, L. S., Gordon, I. E., Barbe, A., Benner, D. C., Bernath, P. F., Birk, M., Boudon, V., Brown, L. R., Campargue, A., Champion, J.-P., Chance, K., Coudert, L. H., Dana, V., Devi, V. M., Fally, S., Flaud, J.-M., Gamache, R. R., Goldman, A., Jacquemart, D., Kleiner, I., Lacome, N., Lafferty, W. J., Mandin, J.-Y., Massie, S. T., Mikhailenko, S. N., Miller, C. E., Moazzen-Ahmadi, N., Naumenko, O. V., Nikitin, A. V., Orphal, J., Perevalov, V. I., Perrin, A., Predoi-Cross, A., Rinsland, C. P., Rotger, M., Šimečková, M., Smith, M. A. H., Sung, K., Tashkun, S. A., Tennyson, J., Toth, R. A., Vandaele, A. C., and Vander Auwera, J.: The HITRAN 2008 molecular spectroscopic database, *J. Quant. Spectrosc. Radiat. Transfer*, 110, 533–572, doi:10.1016/j.jqsrt.2009.02.013, 2009.
- 435
- Sander, R., Kerkweg, A., Jöckel, P., and Lelieveld, J.: Technical note: The new comprehensive atmospheric chemistry module MECCA, *Atmos. Chem. Phys.*, 5, 445–450, doi:10.5194/acp-5-445-2005, 2005.
- 440
- Sander, S. P., Friedl, R. R., Barker, J. R., Golden, D. M., Kurylo, M. J., Wine, P. H., Abbatt, J., Burkholder, J. B., Kolb, C. E., Moortgat, G. K., Huie, R. E., and Orkin, V. L.: *Chemical kinetics and photochemical data for use in atmospheric studies Evaluation no. 17*, JPL Publ. 10-6, Jet Propulsion Laboratory, Pasadena, CA, 2011.
- 445
- Sinnhuber, B.-M., Arlander, D. W., Bovensmann, H., Burrows, J. P., Chipperfield, M. P., Enell, C. F., Frieß, U., Hendrick, F., Johnston, P. V., Jones, R. L., Kreher, K., Mohamed-Tahrin, N., Müller, R., Pfeilsticker, K., Platt, U., Pommereau, J.-P., Pundt, I., Richter, A., South, A. M., Tørnkvist, K. K., Van Roozendaal, M., Wagner, T., and Wittrock, F.: Comparison of measurements and model calculations of stratospheric bromine monoxide, *J. Geophys. Res.*, 107(D19), 4398, doi:10.1029/2001JD000940, 2002.
- 450



- 455 Sinnhuber, B.-M., Sheode, N., Sinnhuber, M., Chipperfield, M. P., and Feng, W.: The contribution of anthropogenic bromine emissions to past stratospheric ozone trends: a modelling study, *Atmos. Chem. Phys.*, 9, 2863–2871, doi:10.5194/acp-9-2863-2009, 2009.
- Sinnhuber, B.-M., and Meul, S.: Simulating the impact of emissions of brominated very short lived substances on past stratospheric ozone trends, *Geophys. Res. Lett.*, 42, 2449-2456, doi:10.1002/2014GL062975, 2015.
- 460 Stiller, G. P., von Clarmann, T., Funke, B., Glatthor, N., Hase, F., Höpfner, M., and Linden, A.: Sensitivity of trace gas abundances retrievals from infrared limb emission spectra to simplifying approximations in radiative transfer modeling, *J. Quant. Spectrosc. Radiat. Transfer*, 72(3), 249-280, 2002.
- Stolarski, R. S., Douglass, A. R., Newman, P. A., Pawson, P., and Schoeberl, M. R.: Relative contribution of greenhouse gases and ozone-depleting substances to temperature trends in the stratosphere: A Chemistry-Climate Model study, *J. Clim.*, 23, 28–42, 2010.
- 465 Tikhonov, A.: On the solution of incorrectly stated problems and a method of regularization, *Dokl. Acad. Nauk SSSR*, 151, 501–504, 1963.
- van Aalst, M. K.: Dynamics and Transport in the Stratosphere - simulations with a general circulation model, Ph.D. thesis, Institute for Marine and Atmospheric Research Utrecht, The Netherlands, 2005.
- 470 Wagner, G., and Birk, M.: New infrared spectroscopic database for chlorine nitrate, *J. Quant. Spectrosc. Radiat. Transfer*, 82, 443-460, 2003.
- Wagner, G., and Birk, M.: New infrared spectroscopic database for bromine nitrate, *J. Mol. Spectrosc.*, 326, 95-105, 2016.
- 475 Warwick, N. J., Pyle, J. A., Carver, G. D., Yang, X., Savage, N. H., O'Connor, F. M., and Cox, R. A.: Global modeling of biogenic bromocarbons, *J. Geophys. Res.*, 111, D24305, doi:10.1029/2006JD007264, 2006.
- 480 Wetzel, G., Oelhaf, H., Kirner, O., Friedl-Vallon, F., Ruhnke, R., Ebersoldt, A., Kleinert, A., Maucher, G., Nordmeyer, H., and Orphal, J.: Diurnal variations of reactive chlorine and nitrogen oxides observed by MIPAS-B inside the January 2010 Arctic vortex, *Atmos. Chem. Phys.*, 12, 6581-6592, doi:10.5194/acp-12-6581-2012, 2012.



485 Wetzels, G., Oelhaf, H., Birk, M., de Lange, A., Engel, A., Friedl-Vallon, F., Kirner, O.,
Kleinert, A., Maucher, G., Nordmeyer, H., Orphal, J., Ruhnke, R., Sinnhuber, B.-M., and
Vogt, P.: Partitioning and budget of inorganic and organic chlorine species observed by
MIPAS-B and TELIS in the Arctic in March 2011, Atmos. Chem. Phys., 15, 8065-8076,
doi:10.5194/acp-15-8065-2015, 2015.



490 **Table 1.** Overview of MIPAS balloon flights and number of limb sequences recorded around sunrise (Kiruna) and sunset (Timmins). Measurement times are given in UTC and local solar time (LST) together with the solar zenith angle (SZA). Latitude and Longitude refer to the tangent points of the observations.

Location	Date	UTC	LST	SZA (deg)	# Seq.	Latitude (°N)	Longitude (°E)
Kiruna	24 Jan 2010	06:17 – 10:21	08:13 – 12:36	98.1 – 86.2	19	69.3 – 66.9	28.8 – 33.7
Kiruna	31 Mar 2011	02:00 – 04:38	04:01 – 06:34	99.4 – 83.1	12	64.0 – 63.5	30.1 – 28.9
Timmins	7/8 Sep 2014	21:40 – 02:33	16:25 – 21:00	69.9 – 115.1	37	45.9 – 46.2	-78.8 – -83.2

495

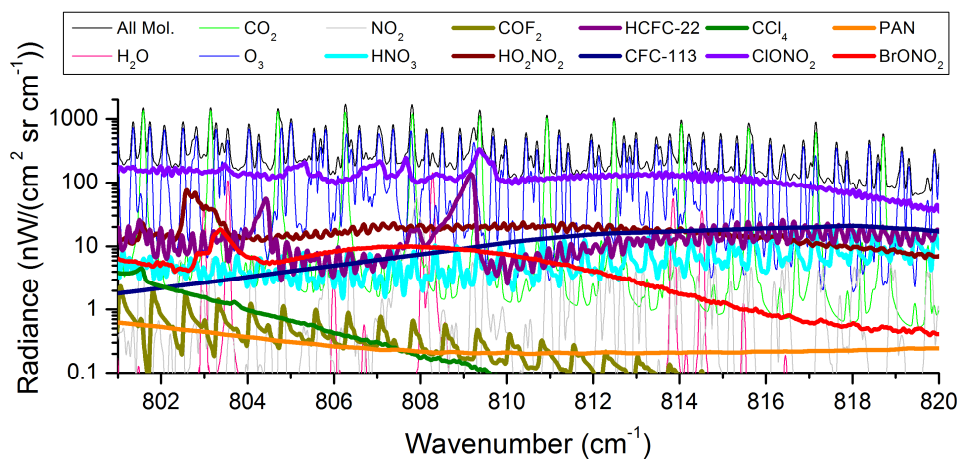


Figure 1. Simulated limb emission spectra (with spectral resolution of MIPAS-B) for a mid-latitude summer standard atmosphere (Remedios et al., 2007) in the spectral region of the BrONO₂ analysis window for a tangent altitude of 20 km. Emissions of individual species contributing to the combined spectrum (all molecules, black line) are shown.

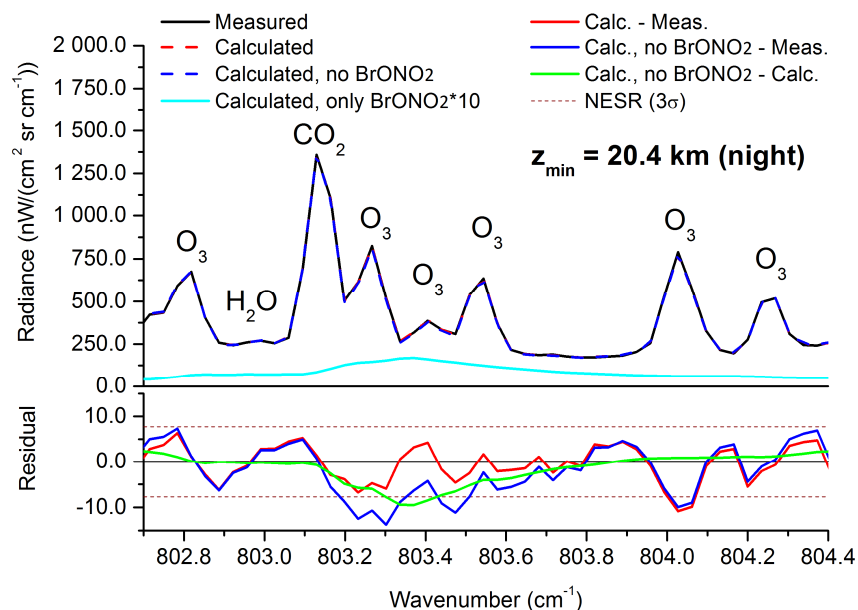


Figure 2. Top panel: Best fit of measured spectrum (black solid line) zoomed around the Q-branch of the BrONO_2 ν_3 fundamental band at 803.37 cm^{-1} for a tangent altitude (z_{min}) near 20 km recorded during night on 7/8 September 2014 above Timmins (Seq. 05a). A calculation with (red dashed line) and without (blue dashed line) BrONO_2 in the model atmosphere was performed. The calculated individual emission of the BrONO_2 band (scaled by a factor of 10; cyan solid line) is shown, too. Bottom panel: Difference between the calculated and measured spectrum (red solid line); difference between the calculated spectrum (without BrONO_2) and the measured one (blue solid line); difference of both calculations (green solid line). The $3\text{-}\sigma$ NESR (brown dotted line) is displayed, too.

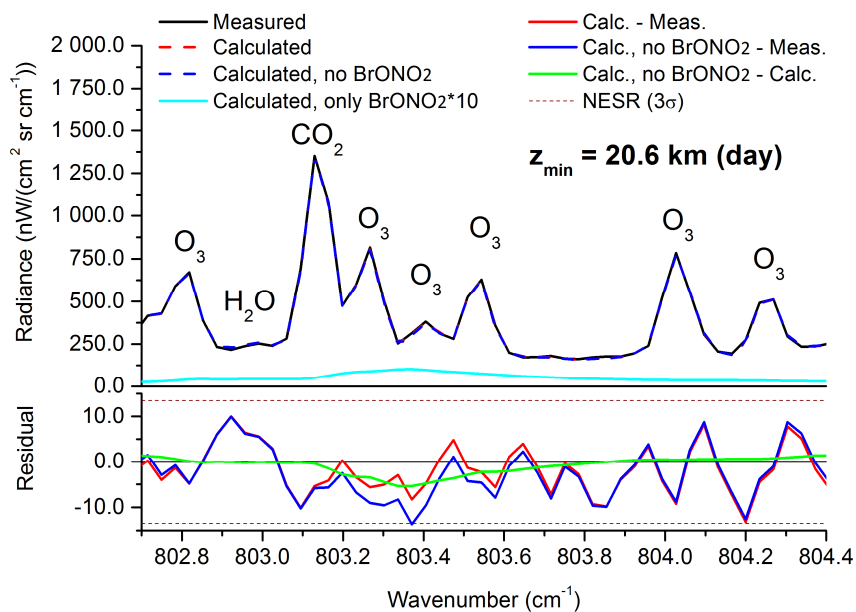


Figure 3. Same as Figure 2 but for a spectrum observed during day (Seq. 02e). The difference between the red and blue solid line (bottom panel) is smaller than the corresponding nighttime difference shown in Figure 2. Hence, BrONO₂ amounts seen during day are lower than the ones observed at night.

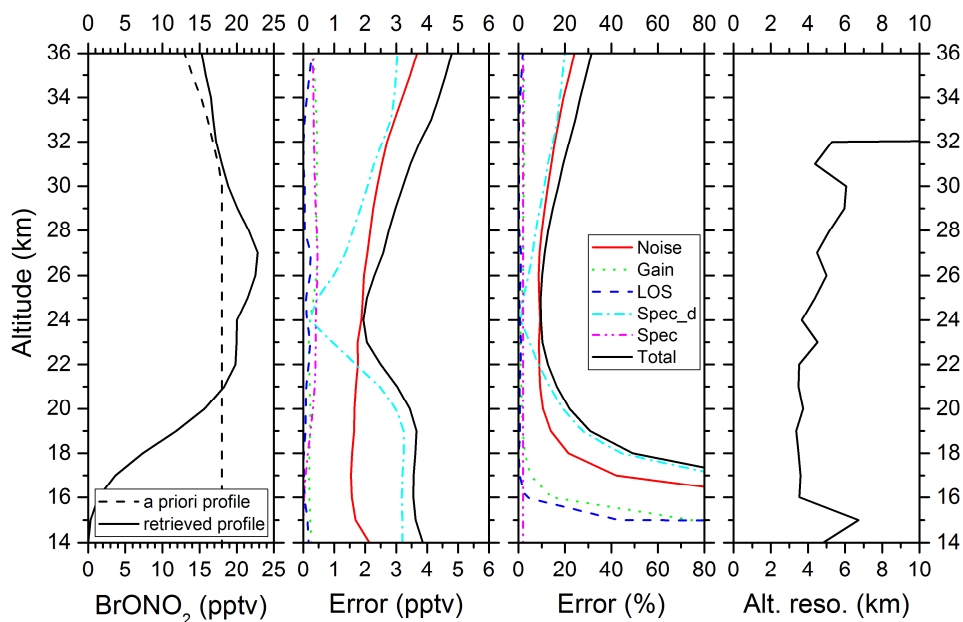


Figure 4. Retrieved BrONO₂ VMR vertical profile (and a priori profile) for a nighttime (Seq. 05a) limb sequence recorded by MIPAS-B on 7/8 September 2014 above Timmins together with absolute and relative errors and the altitude resolution, determined from the full width at half maximum of the columns of the averaging kernel matrix. The following error contributions are shown: spectral noise (red solid line), radiometric gain (green dotted line), LOS (blue dashed line), spectroscopic data of disturbing gases (dash dotted cyan line), spectroscopic data of target molecule BrONO₂ (short dash dotted magenta line), and total error (black solid line).

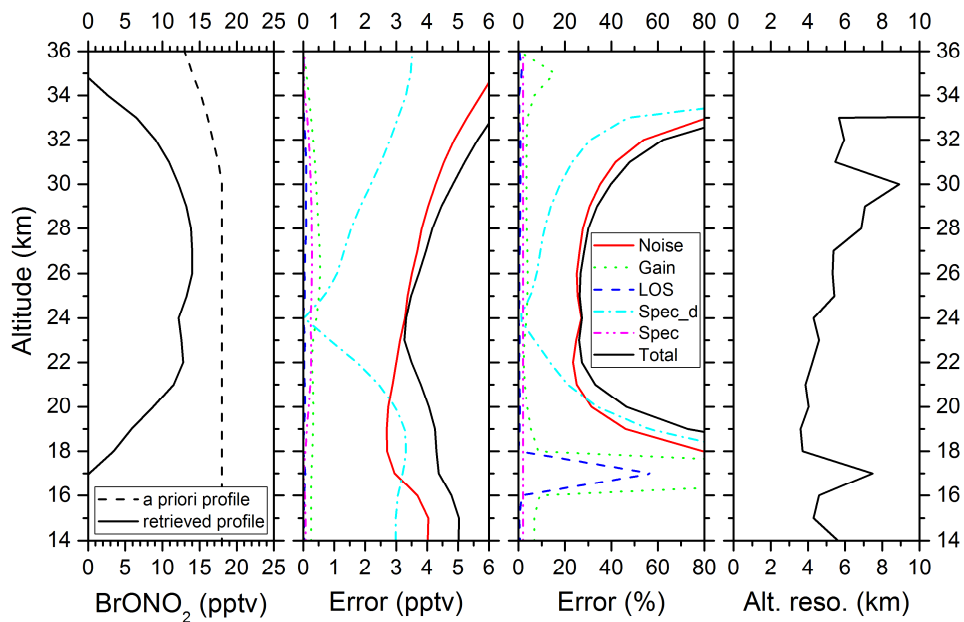


Figure 5. Same as Figure 4 but for a limb sequence measured during day (Seq. 02e).

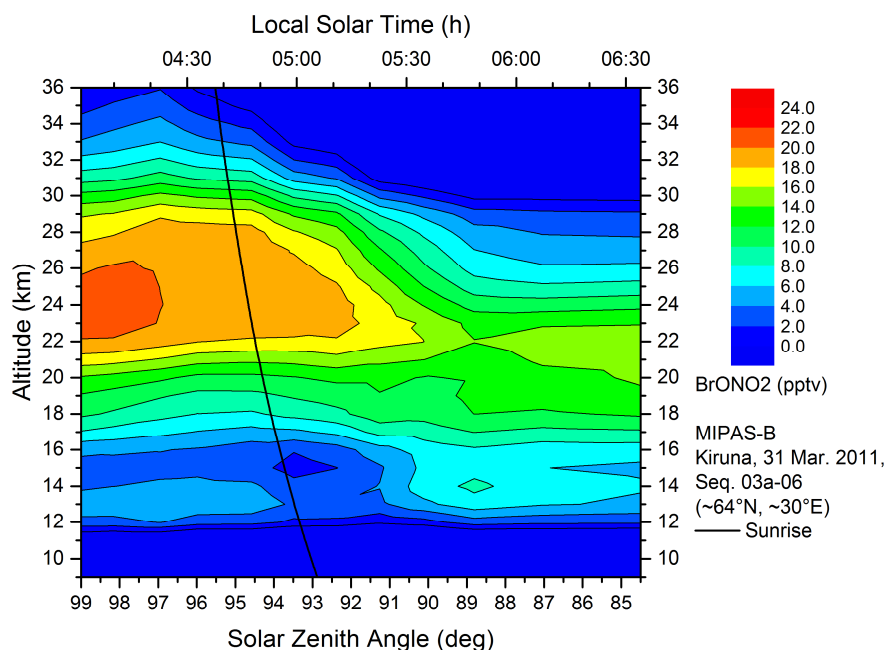


Figure 6. Temporal evolution of BrONO₂ volume mixing ratios (pptv) as seen by MIPAS-B from a float altitude around 35 km above northern Scandinavia on 31 March 2011 inside the late winter Arctic vortex. The black solid line marks the sunrise terminator. A decrease in the BrONO₂ amount starting around sunrise is clearly visible.

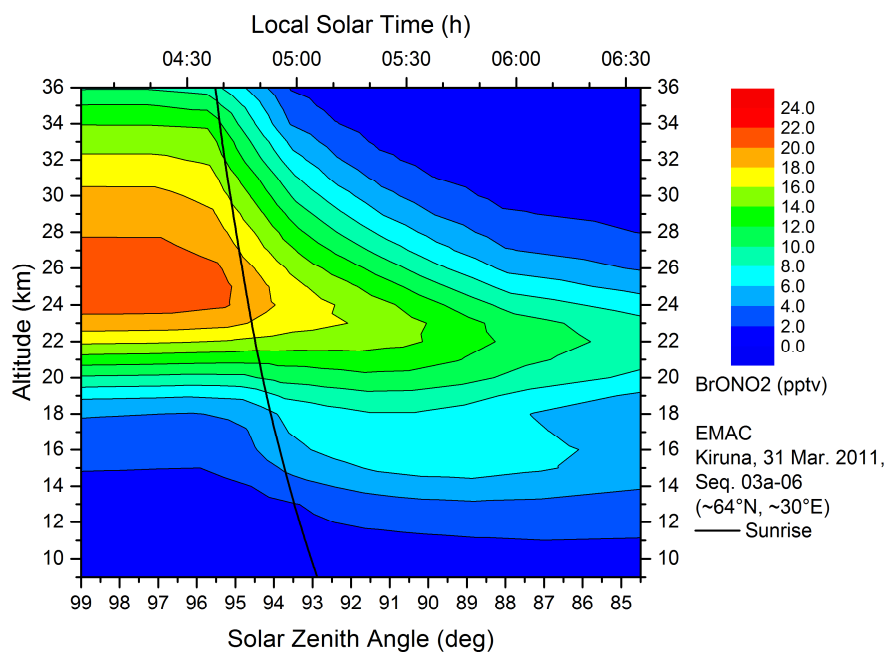


Figure 7. Temporal evolution of BrONO₂ on 31 March 2011 as simulated by the chemistry climate model EMAC. The decrease of BrONO₂ starts close to sunrise.

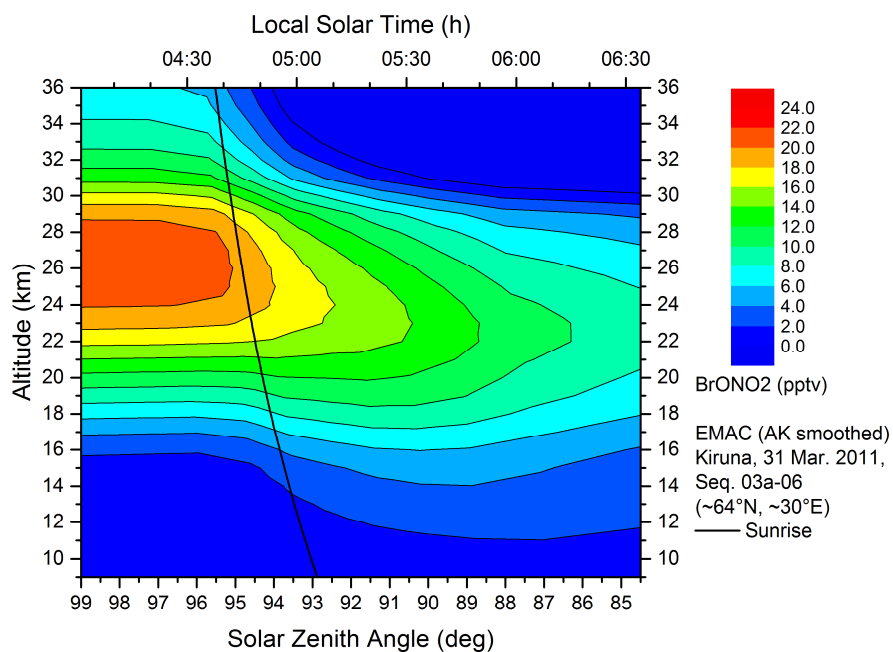


Figure 8. Same as Figure 7 but EMAC vertical profiles smoothed with the MIPAS-B averaging kernel (AK).

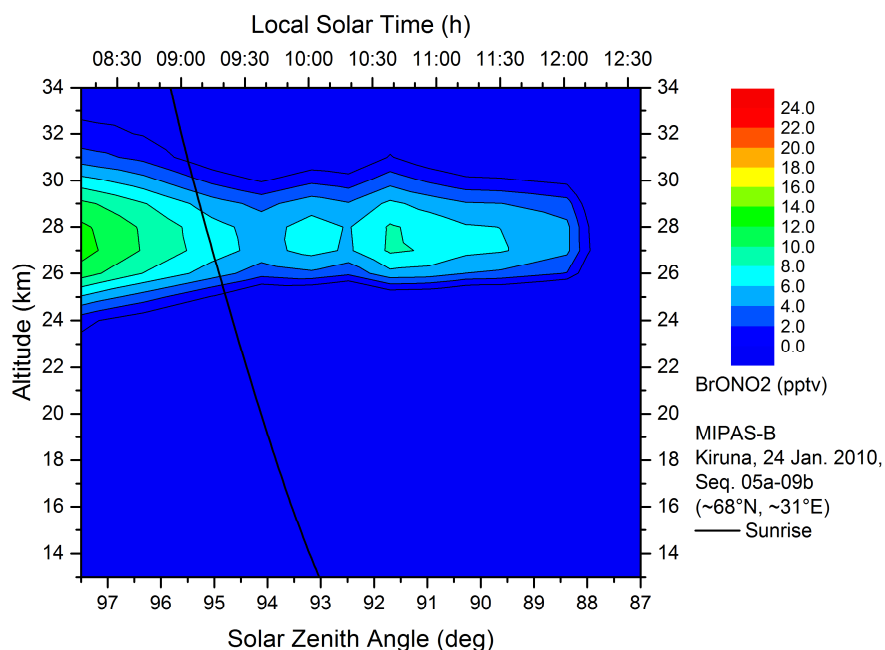


Figure 9. Temporal evolution of BrONO₂ volume mixing ratios (pptv) as measured by MIPAS-B on 24 January 2010 inside the mid-winter Arctic vortex (observer altitude about 34 km). The black solid line marks the sunrise terminator. The still weak illumination at the end of the polar night is responsible for the small diurnal variation of the BrONO₂ amount.

505

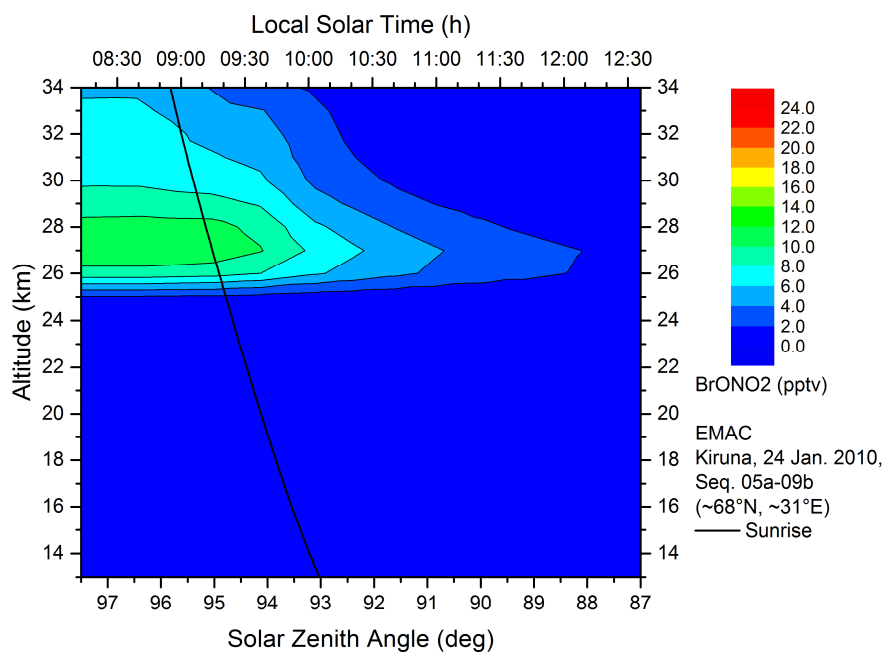


Figure 10. Temporal evolution of BrONO₂ on 24 January 2010 as simulated by the chemistry climate model EMAC. The decrease of BrONO₂ starts close to sunrise.

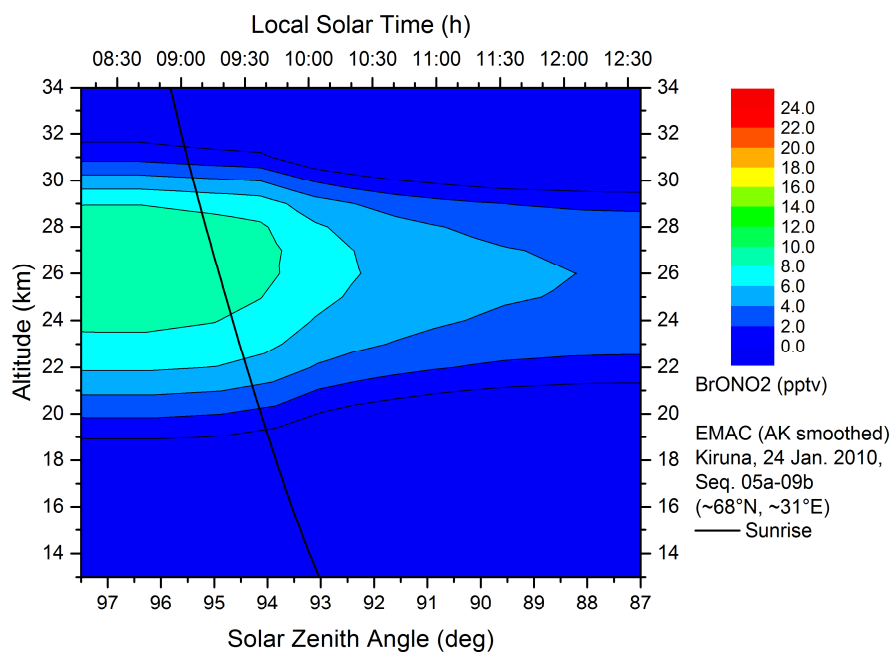


Figure 11. Same as Figure 10 but EMAC vertical profiles smoothed with the MIPAS-B averaging kernel (AK).

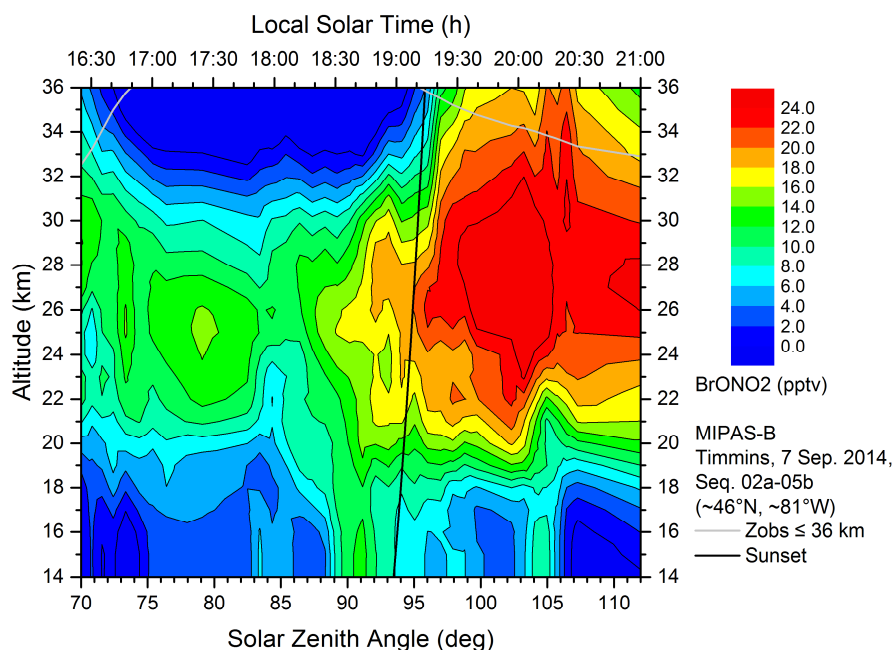


Figure 12. Temporal evolution of BrONO₂ amounts observed by MIPAS-B near 46°N above Ontario (Canada) on 7 September 2014. The grey line indicates the time periods where the balloon gondola float altitude was lower or equal to 36 km. The black solid line marks the sunset terminator. The build-up of BrONO₂ from daytime BrO starts shortly before sunset.

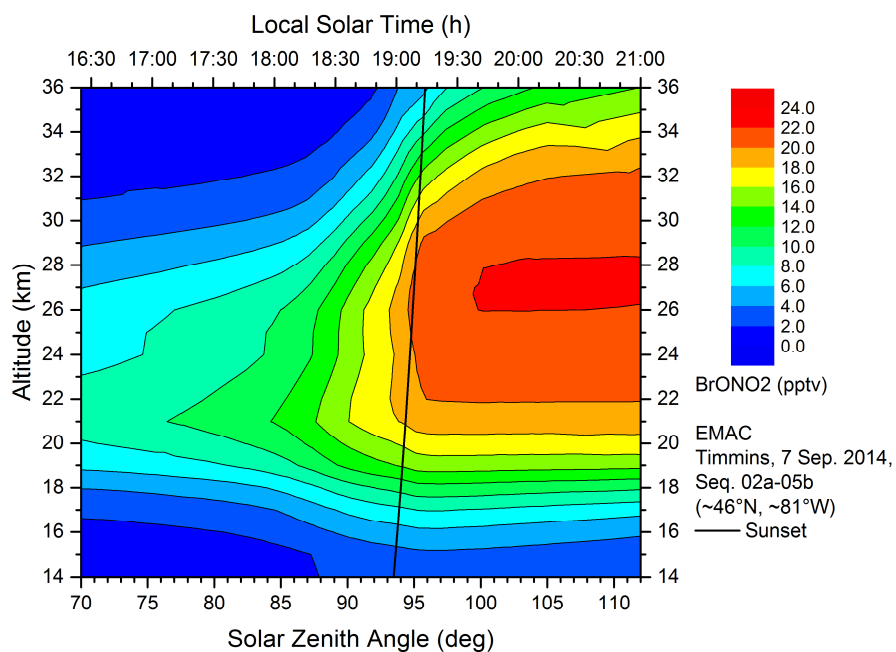


Figure 13. Temporal evolution of BrONO₂ on 7 September 2014 as simulated by the EMAC model.

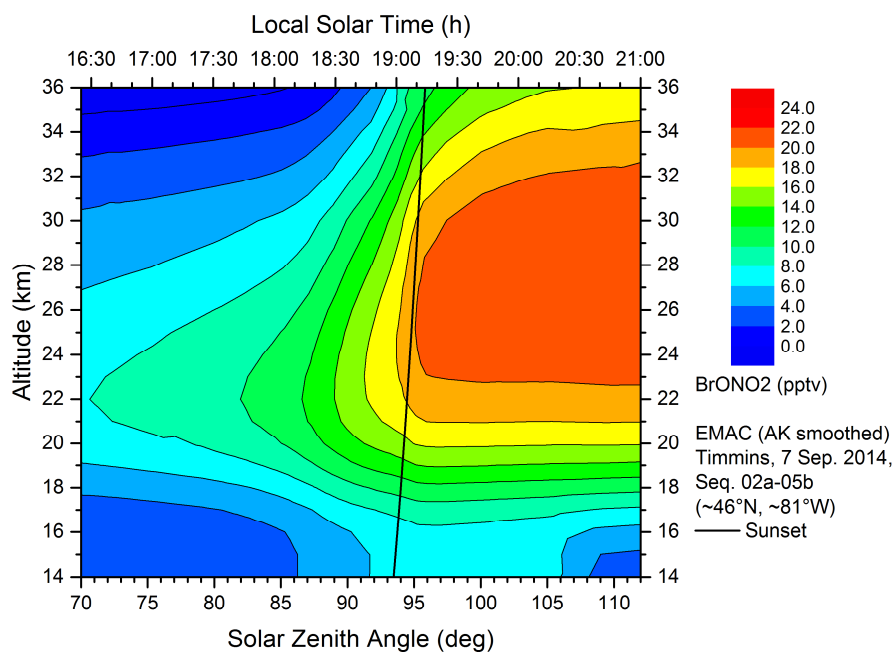


Figure 14. Same as Figure 13 but EMAC vertical profiles smoothed with the MIPAS-B averaging kernel (AK).

510